



Application of the Direct Power Control Strategy in a Shunt Active Filter by Exploiting the Solar Photovoltaic Energy as a Continuous Source

A. Morsli¹, A. Tlemçani^{1*}, A. Krama², A. Abbadi¹, L. Zellouma²
and H. Nouri³

¹ *Electrical Engineering and Automation Research Laboratory (LREA), University of Medea, 26000, Medea, Algeria.*

² *Saharan Energy Resources Exploitation and Valorization Laboratory (LEVRES) of El-Oued, B.P. 789 El-Oued 39000, Algeria.*

³ *Power Systems, Electronics and Control Research Group, Department of Engineering Design and Mathematics, University of West of England, Bristol, BS16 1QY, U.K.*

Received: January 11, 2020; Revised: October 1, 2020

Abstract: In order to follow the standard recommendations of the electrical energy quality (IEEE519) on the distribution network, the active filters have responded to these recommendations, which require that the Total Harmonic Distortion (THD) must be less than 5%. The purpose of this paper is to improve the waveform of the electric current that is distorted due to the non-linear load by the shunt active filtering system by exploiting photovoltaic solar energy as a source of the continuous bus of the inverter and obtain a waveform of the sinusoidal source current with a THD in accordance with the recommendations cited above. To show what we have said, we used a SAPF powered by a PV system (module type MSX120 and a DC-DC boost converter controlled by the (P and O) method) controlled by the Direct Power Control (DPC) technique. The simulation results under *MATLAB/Simulink* showed us the effectiveness of the proposed system.

Keywords: *direct power control (DPC); perturbation and observation (P and O); photovoltaic solar system; shunt active power filter (SAPF).*

Mathematics Subject Classification (2010): 93C42, 03B52, 93E11, 93Cxx.

* Corresponding author: mailto:h_tlemcani@yahoo.fr

1 Introduction

The shunt active power filter is powered by a DC voltage source or a capacitor which is expensive. Our paper proposes another free continuous source by the sun, it is the photovoltaic solar energy which transforms the light energy into electrical energy via the PV sensor.

Fig. 1 shows the principle schematics of the SAPF.

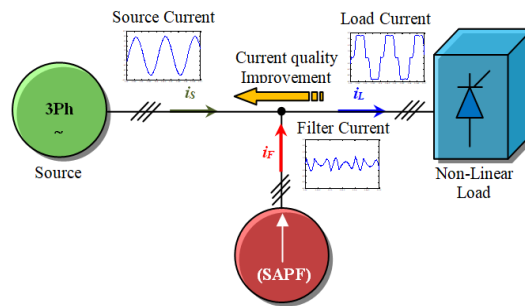


Figure 1: Principle Schematics of the Shunt Active Power Filter.

In this paper, the supply of the SAPF is provided by a photovoltaic solar module as a clean and free source. In order to output active power in the electrical network lines, it guarantees the harmonics compensation of the source current and a reduced cost of the SAPF. The regulation of the voltage of the PV system allowed us to obtain the reference of the active power by means of a PI regulator. Thus, the MPPT command by the (P and O) controller of the Boost converter is made to maintain the output voltage of the PV module constant and to follow the reference value. The three-phase two-level inverter is controlled by the DPC technique which is based on hysteresis comparators using a switchboard. This control approach shows a significant difference in terms of dynamics, robustness and stability compared to the traditional P-Q method.

2 The Photovoltaic Solar System

Fig. 2 shows the photovoltaic system which supplies the shunt active filter by a delivered voltage V_{dc} which is equal to 96 V.

2.1 Modeling of photovoltaic module

The basic element of each photovoltaic system is the photovoltaic module. It has PV cells connected together [1–3]. The PV modules are of type BP-MSX120, their characteristics are given in Tab. 1.

For PV solar module modeling, we applied the frequently used model to describe the electrical characteristics of this module which takes into account the different internal resistances (Fig. 3) [4, 5].

The equivalent circuit mathematical expression of the PV module is presented by

$$I_{PV} = I_{ph} - I_D - I_R, \tag{1}$$

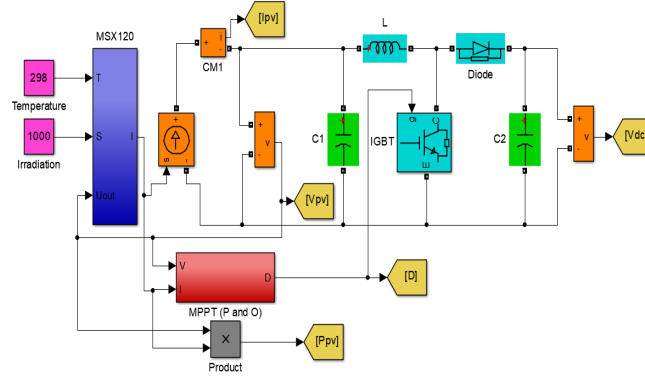


Figure 2: PV solar system (Panel, Boost converter and MPPT).

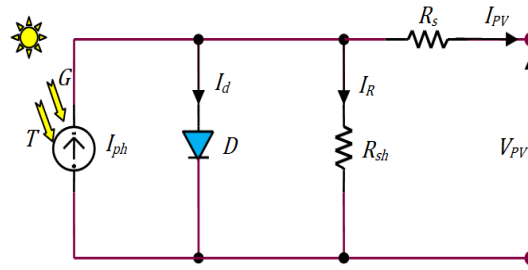


Figure 3: Equivalent circuit of a PV solar module.

$$I_{PV} = I_{ph} - I_0 \left[\exp \left(\frac{q(V_{PV} + z \cdot R_s \cdot I_{PV})}{z \cdot n \cdot k \cdot T_{ck}} \right) - 1 \right] - \frac{V_{PV} + z \cdot R_s \cdot I_{PV}}{z \cdot R_{sh}}. \quad (2)$$

Or,

I_{PV} : PV current [A],

I_{ph} : Photo-current [A],

I_0 : Reverse saturation current [A],

q : Electron charge

$$q = 1.6 \cdot 10^{-19} \text{ coulomb}$$

V_{PV} : PV Voltage [V],

z : Number of cells in series,

R_s : Series resistance [Ω],

R_{sh} : Shunt resistance [Ω],

n : Ideality factor varies between 1 and 2,

k : constant of Boltzmann

$$k = 1.38 \cdot 10^{-23} \text{ J} \cdot \text{K}^{-1}$$

BP SOLAR MSX 120	
Maximum Power Point P_{max}	120 W
Voltage at P_{max} V_{mp}	33.7 V
Current at P_{max} I_{mp}	3.56 A
Open-circuit voltage V_{oc}	42.1 V
Short-circuit current I_{sc}	3.87 A
Series resistance R_s	0.473 Ω
Shunt resistance R_{sh}	1367 Ω
Ideality factor n	1.3977
Temperature coefficient of I_{sc} k_i	(0.065 \pm 0.015)%/C
Temperature coefficient of V_{oc} k_v	– (80 \pm 10) mV/C
Temperature coefficient of P_{max} k_p	– (0.5 \pm 0.05)%/C
NOCT	(47 \pm 2)C
Number of cells connected in series n_s	72

Table 1: Datasheet parameters of the PV module.

2.2 Modeling of DC-DC converter and MPPT controller

In order to guarantee the level of voltage required to supply the shunt active power filter, the voltage delivered by the PV module is insufficient ($V_{PV} = 42.1$ V), while the inverter must supply a voltage greater than V_{PV} . For this, we used a DC-DC boost converter (Fig. 4) [8].

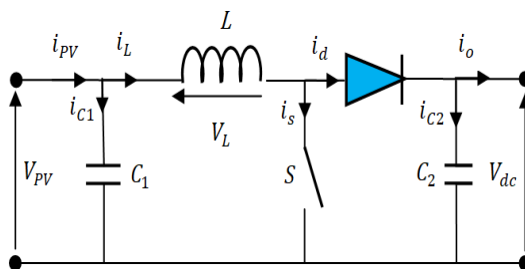


Figure 4: Ideal circuit of boost converter.

The following equations are obtained from Fig. 3 when the switch S is open.

$$i_{c1}(t) = C_1 \frac{dv_{PV}(t)}{dt} = i_{PV}(t) - i_L(t), \tag{3}$$

$$i_{c2}(t) = C_2 \frac{dv_{dc}(t)}{dt} = i_L(t) - i_o(t), \tag{4}$$

$$v_1(t) = L \frac{di_L(t)}{dt} = v_{PV}(t) - v_{dc}(t). \tag{5}$$

This transistor controlled by the (P and O) algorithm aims to tracking the maximum power point MPPT. The latter is then controlled using a MPPT controller with the Perturbation and Observation (P and O) algorithm, as shown in Fig. 5.

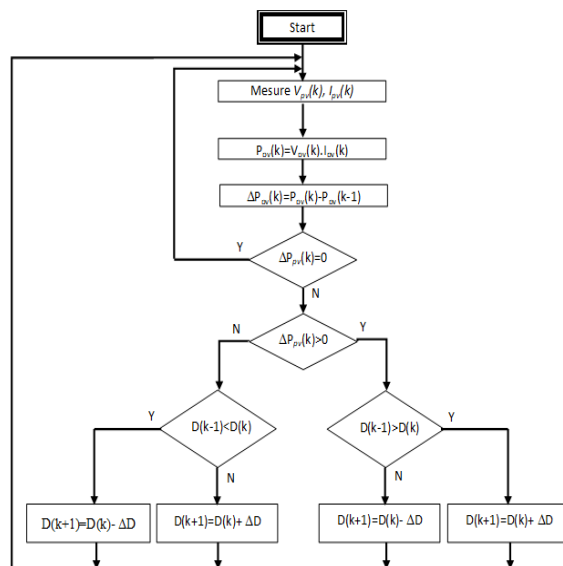


Figure 5: Perturbation and Observation algorithm [9].

The switch S is a MOSFET transistor and internal diode in parallel with a series RC snubber circuit. When a gate signal is applied, the MOSFET conducts and acts as a resistance (R_{on}) in both directions. If the gate signal falls to zero when current is negative, current is transferred to the antiparallel diode. Their parameters are shown in Tab. 2.

MOSFET Transistor	
FET resistance R_{on}	0.1 Ω
Internal diode inductance L_{on}	0 H
Internal diode resistance R_d	0.01 Ω
Internal diode forward voltage V_f	0 V

Table 2: MOSFET Transistor parameters [10].

3 Modeling of Shunt Active Power Filter

Recently, there are fast switching power devices controlled by different strategies. These devices can compensate the harmonics due to the nonlinear charge by producing counter-harmonic currents [11]. The used SAPF is an inverter with two levels of IGBT Transistor and internal diode in parallel. Their parameters are shown in Tab. 3.

IGBT Transistor	
IGBT resistance R_{on}	0.001 Ω
Snubber resistance R_s	100000 Ω
Snubber capacitance C_s	Inf F

Table 3: IGBT Transistor parameters [10].

The work of the simulation model is as follows:

- Mainly the circuit consists of an inverter which consists of 6 IGBTs.
- The inverter is basically used to convert DC into AC. The input of the inverter is 96V dc and the output is connected between the supply network and non linear load through the RL filter in order to inject the filter current i_f .

The simple voltages of the three phases a, b and c at the output of the inverter are given as follows:

$$v_{fa} = V_{An} = 2U_c \frac{2S_a - S_b - S_c}{3} = V_{dc} \frac{2S_a - S_b - S_c}{3}, \tag{6}$$

$$v_{fb} = V_{Bn} = 2U_c \frac{2S_b - S_a - S_c}{3} = V_{dc} \frac{2S_b - S_a - S_c}{3}, \tag{7}$$

$$v_{fc} = V_{Cn} = 2U_c \frac{2S_c - S_a - S_b}{3} = V_{dc} \frac{2S_c - S_a - S_b}{3}. \tag{8}$$

Thus, we can express eight possible cases of the output voltage of the active filter V_{fk} (referred to the neutral N of the source) as shown in Tab. 4 [12].

Case	S_a	S_b	S_c	v_{fa}/V_{dc}	v_{fb}/V_{dc}	v_{fc}/V_{dc}
0	0	0	0	0	0	0
1	1	0	0	2/3	-1/3	-1/3
2	0	1	0	-1/3	2/3	-1/3
3	1	1	0	1/3	1/3	-2/3
4	0	0	1	-1/3	-1/3	2/3
5	1	0	1	1/3	-2/3	1/3
6	0	1	1	-2/3	1/3	1/3
7	1	1	1	0	0	0

Table 4: Possible voltages in the output of the inverter.

The structure of inverter is shown in Fig. 6.

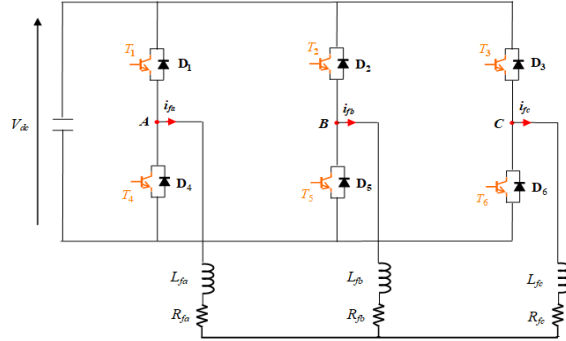


Figure 6: Structure of the three-phase inverter with two levels [13].

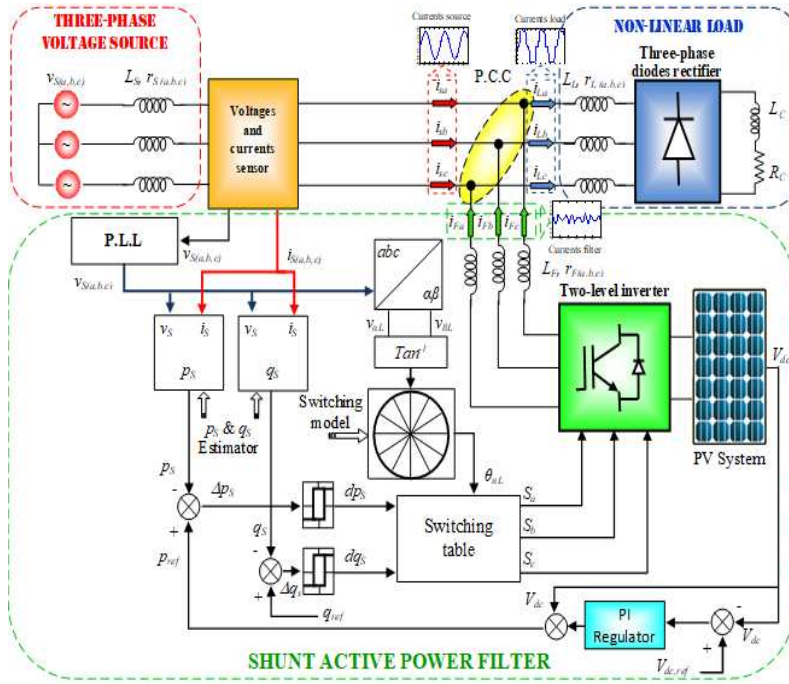


Figure 7: Block diagram of the SAPF controlled by the DPC connected with a PV solar panel.

3.1 Direct power control (DPC) technique

Fig. 7 shows the system of a shunt active power filtering controlled by the DPC technique and connected with a solar photovoltaic panel.

These powers are expressed, respectively, by the following relations [10, 12, 14]:

$$p_s(t) = v_{sa} \cdot i_{sa} + v_{sb} \cdot i_{sb} + v_{sc} \cdot i_{sc}, \quad (9)$$

$$q_s(t) = \frac{1}{\sqrt{3}} [(v_{sb} - v_{sc}) \cdot i_{sa} + (v_{sc} - v_{sa}) \cdot i_{sb} + (v_{sa} - v_{sb}) \cdot i_{sc}]. \quad (10)$$

For this purpose, the stationary coordinates are divided into 12 sectors, as shown in Fig. 8. The digitized signal errors d_{ps} , d_{qs} and voltage phase θ_n are the inputs of switching table shown in Table 1 whose output is the switching state (S_a, S_b, S_c) of the converter. By using this switching table, the optimal state of the converter can be selected uniquely during each time interval according to the combination of the table inputs. The selection of the optimal switching state is performed so that the power errors can be restricted within the hysteresis bands [10, 15].

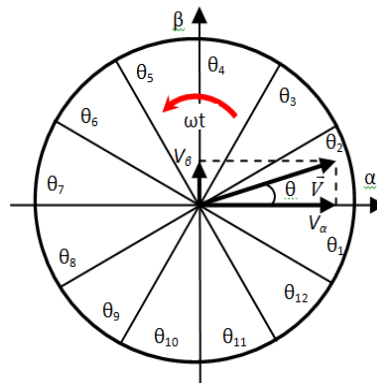


Figure 8: (α, β) twelve (12) sectors representation.

The digitized variables d_{ps} , d_{qs} and grid voltage vector position θ (equation (11)), form a digital word, for access to the address of switching table select the appropriate control voltage vector

$$\theta = \arctan \frac{v_\beta}{v_\alpha}. \tag{11}$$

Determination of the number of sector is given by

$$(n - 2) \frac{\pi}{6} < \theta_n < (n - 1) \frac{\pi}{6}, \tag{12}$$

where n indicates the sector number ($n = 1, 2, \dots, 12$) [10, 16]. The input voltage can be estimated by the following equation:

$$\begin{bmatrix} v_\alpha \\ v_\beta \end{bmatrix} = \frac{1}{i_\alpha^2 + i_\beta^2} \begin{bmatrix} i_\alpha & -i_\beta \\ i_\beta & i_\alpha \end{bmatrix} \begin{bmatrix} \hat{p} \\ \hat{q} \end{bmatrix}. \tag{13}$$

The same observation can be made for d_q and even sectors (θ_i), i =even. So, this shows the limits of this switching table DPC (Tab.5) [10, 17]. The knowledge of the estimated voltage sector is necessary to determine optimal switching states.

The conversion in the $\alpha - \beta$ coordinate system by the system voltages with the Concordia transformation gives

$$\begin{bmatrix} v_{s\alpha}(\theta) \\ v_{s\beta}(\theta) \end{bmatrix} = [T_{32}]^t \cdot \begin{bmatrix} v_{sa}(\theta) \\ v_{sb}(\theta) \\ v_{sc}(\theta) \end{bmatrix}. \tag{14}$$

d_p	d_q	θ_1	θ_2	θ_3	θ_4	θ_5	θ_6	θ_7	θ_8	θ_9	θ_{10}	θ_{11}	θ_{12}
1	0	101	111	100	000	110	111	010	000	011	111	001	000
1	1	111	111	000	000	111	111	000	000	111	111	000	000
0	0	101	100	100	110	110	010	010	011	011	001	001	101
0	1	100	110	110	010	010	011	011	001	001	101	101	100

Table 5: Switching sectors of the DPC.

The $d - q$ voltage components are derived by the Park transformation, where $\hat{\theta}$ represents the instantaneous reference voltage vector angle,

$$\begin{bmatrix} v_{sd} \\ v_{sq} \end{bmatrix} = p(\hat{\theta}) \cdot \begin{bmatrix} v_{s\alpha}(\theta) \\ v_{s\beta}(\theta) \end{bmatrix} \quad (15)$$

with

$$p(\hat{\theta}) = \frac{1}{i_{\alpha}^2 + i_{\beta}^2} \begin{bmatrix} \cos \hat{\theta} & \sin \hat{\theta} \\ -\sin \hat{\theta} & \cos \hat{\theta} \end{bmatrix} \quad (16)$$

and after substituting (14) in (16), the voltages v_{sd} and v_{sq} are given by:

$$\begin{bmatrix} v_{sd} \\ v_{sq} \end{bmatrix} = \sqrt{3} \cdot V_m \cdot \begin{bmatrix} \sin(\theta - \hat{\theta}) \\ -\cos(\theta - \hat{\theta}) \end{bmatrix}. \quad (17)$$

4 Simulation Results and Discussions

The simulation of the system made with the *MATLAB/Simulink* environment allowed us to obtain the results below. Fig. 9 shows the voltage delivered by the PV module. We note that this voltage is reached at its open-circuit value which is equal to 42.1 V in a very fast time at time $t = 0.005$ s.

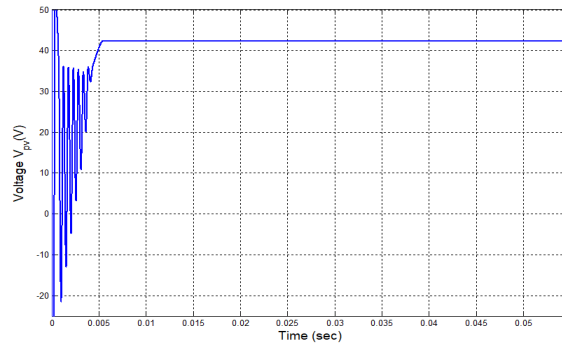


Figure 9: Photovoltaic voltage V_{pv} .

The curves (shown in Fig. 10) express current and power as a function of time. We

observe that the parameters shown in Tab.1 are completed according to the *datasheet* of this module.

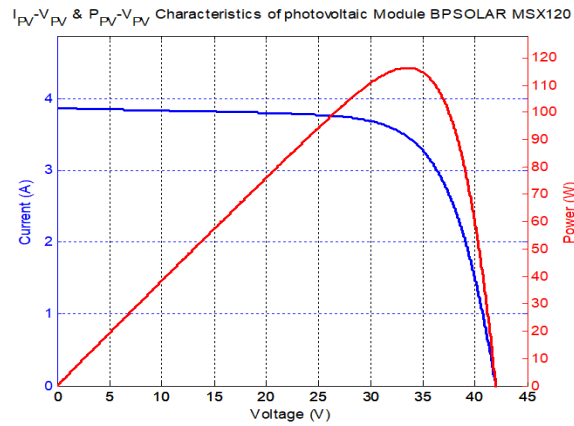


Figure 10: Current I_{pv} and power P_{pv} in the function of voltage V_{pv} for a PV solar module of type BP-MSX120.

Fig. 11 shows the Duty cycle as a function of time. D increases from the value null to the value 0.5 at the instant 0.01 s.

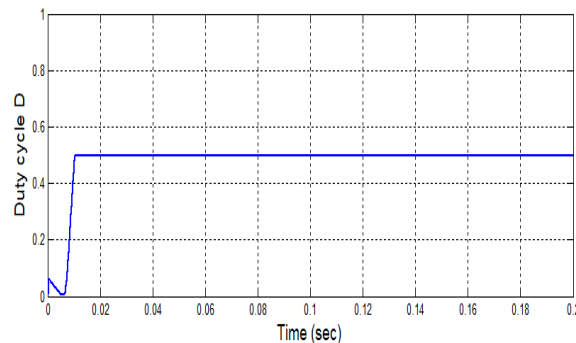


Figure 11: Duty cycle D in the function of time.

Fig. 12 shows the DC link voltage delivered by the boost DC-DC converter. We clearly see that the voltage V_{dc} reaches the reference value which is equal to 96 V at the instant 0.035 s.

Fig. 13 shows the load current delivered by the non-linear load without the SAPF. We see that the signal is distorted because of the harmonics injected by the rectifier with an amplitude value equal to 2.402 A.

Its spectral analysis gives a total harmonic distortion and shows a very high THD to the value accepted by the supply grid which requires a current THD of less than 5%. We see that $THD_{iLa} = 25.32\%$, which is unacceptable. The harmonics that have appeared are of order $(6h \pm 1)$ because of the three-phase source and the non-linear load, i.e., in

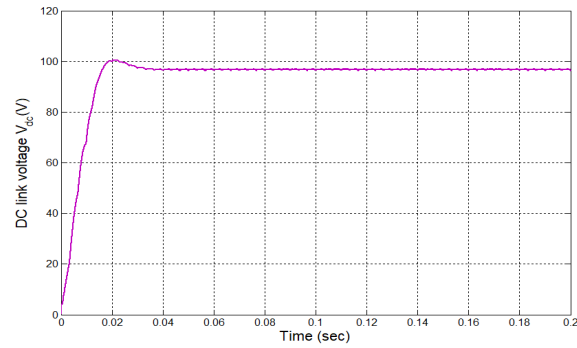


Figure 12: DC link voltage in the output of the boost converter V_{dc} .

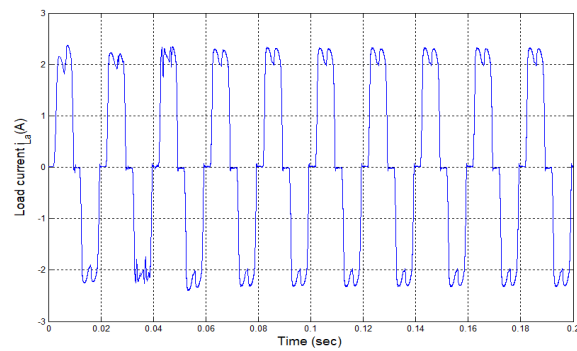


Figure 13: Load current i_{La} without the SAPF.

the range of 30 orders, the order harmonics 5, 7, 11, 13, 17, 19, 23, 25 and 29 appeared (Fig. 14).

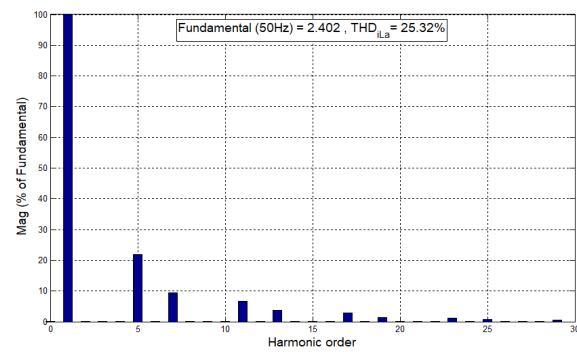


Figure 14: Total Harmonic Distortion of i_{La} .

After connecting the SAPF, we obtained the signal illustrated in Fig. 15. This is the

source current i_{Sa} which becomes almost sinusoidal with an amplitude value equal to 4.412 A.

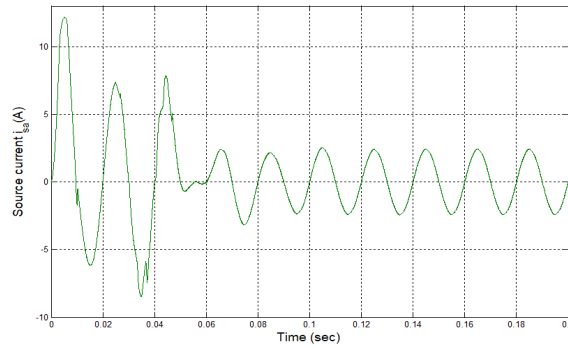


Figure 15: Source current i_{Sa} with the SAPF.

Its spectral analysis gives a THD is less than 5%. We see that $THD_{i_{Sa}} = 2.94\%$, which is acceptable.

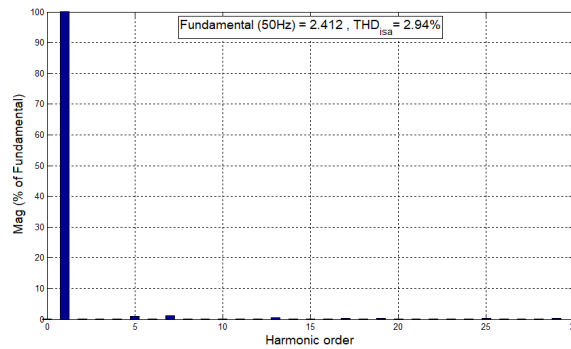


Figure 16: Total Harmonic Distorsion of i_{Sa} .

Fig. 17 shows the filter current i_{Fa} delivered by the SAPF.

Fig. 18 shows the system currents in same figure. The filter current i_{Fa} delivered by the SAPF which compensates for the load current i_{La} by the following formula:

$$i_{Sa} = i_{La} - i_{Fa}. \tag{18}$$

Fig. 19 represents the active P_s and its reference P_s^* powers. This shows us that the active power follows its reference which is equal to 200 W at permanent regime after closing the switch placed between the shunt active filter and the line.

Fig. 20 represents the reactive Q_s and its reference Q_s^* powers. This shows us that the reactive power follows its reference which is equal to 0 VAR at permanent regime after closing the switch placed between the shunt active filter and the line.

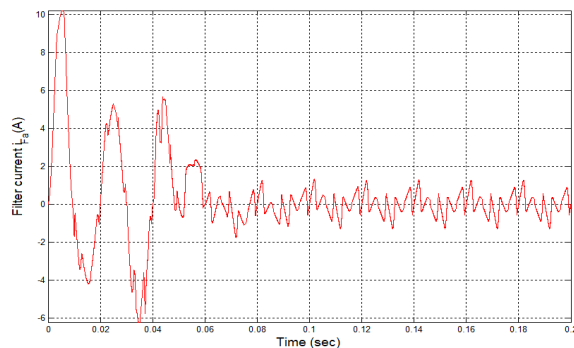


Figure 17: Filter current i_{Fa} .

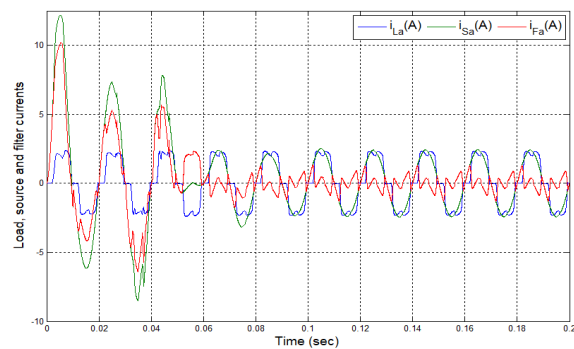


Figure 18: Load, source and filter currents i_{La} , i_{sa} and i_{Fa} .

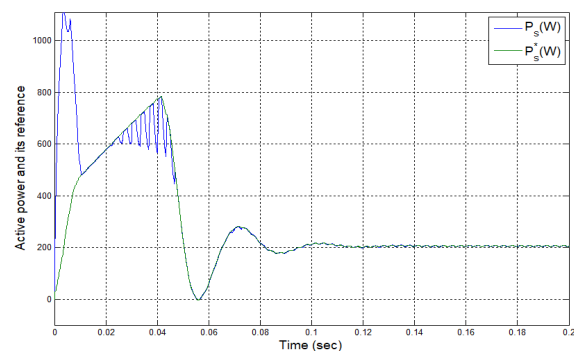


Figure 19: Active power P_s and its reference P_s^* .

5 Conclusion

The harmonics injected into the electricity grid by the nonlinear charges pollute the lines of this network, which causes the deformation of the electric currents on the one

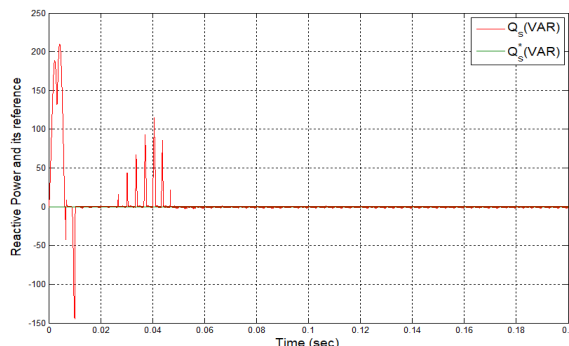


Figure 20: Reactive power Q_s and its reference Q_s^* .

hand and the malfunction of the electrical appliances on the other hand. To clean up the supply network, several methods have been proposed between liabilities and assets. Our proposal is parallel active filtering controlled by the Direct Power Control (DPC) technique. The DC bus is powered by a photovoltaic source. The simulation results under *MATLAB/Simulink* show us that the filter has improved the quality of electrical energy, and especially the wave of electric current i_{Sa} source. We clearly see that:

1. $THD_{iLa}=25.32\%$ before filtering decreased to $THD_{iSa}=2.94\%$ after filtering;
2. The SAPF i_{La} current compensated the reagent in the feed lines;
3. The active and reactive powers have followed their references.

Finally, we can say that the application of the PV system in parallel active filters has a better harmonic compensation performance and reactive power.

References

- [1] K. Ishaque, Z. Salam, H. Taheri and S. Syafaruddin. Modeling and Simulation of Photovoltaic PV System During Partial Shading Based on a Two-Diode Model. *Simulation Modeling Practice and Theory* **19** (07) (2011) 1613–1626.
- [2] K. Ishaque, Z. Salam and S. Syafaruddin. A Comprehensive MATLAB Simulink PV System Simulator with Partial Shading Capability Based on Two-Diode Model. *Solar Energy* **85** (09) (2011) 2217–2227.
- [3] N. Belhaouas, M. S. Ait-Cheikh, A. Malek and C. Larbes. Matlab-Simulink of photovoltaic system based on a two-diode model simulator with shaded solar cells. *Revue des Energies Renouvelables* **16** (01) (2013) 65–73.
- [4] A. Hoque and K. A. Wahid. New Mathematical Model of a Photovoltaic Generator PVG. *Bangladesh Journal of Electrical Engineering* **28** (01) (2000).
- [5] A. Hansen, P. Sorensen, L. Hansen and H. Bindner. Models for Stand-Alone PV System. *Riso National Laboratory, Roskilde, Denmark*, ISBN 87-550-2774-1.
- [6] A. S. Golder. Photovoltaic Generator Modeling for Large Scale Distribution System Studies. *Thesis Master of Science in Electrical Engineering*. October, 2006.

- [7] A. Morsli. Etude d'un système solaire photovoltaïque utilisant des supercondensateurs. *Mémoire de Magistère en électricité solaire. Ecole Nationale Polytechnique ENP, Algeria*, 2010.
- [8] A. Krama, L. Zellouma and B. Rabhi. Improved Control of Shunt Active Power Filter Connected to a Photovoltaic System Using Technique of Direct Power Control. In: *8th International Conference on Modelling, Identification and Control ICMIC2016*, Algiers, Algeria. November 15 – 17, 2016.
- [9] F. Hamidia, A. Abbadi, A. Tlemçani and M. S. Boucherit. Dual star induction motor supplied with double photovoltaic panels based on fuzzy logic type-2. *Nonlinear Dynamics and Systems Theory* **18** (04) (2018) 359–371.
- [10] A. Morsli, A. Tlemçani and M. S. Boucherit. Shunt Active Power Filter Based Harmonics Compensation of a Low-Voltage Network Using Fuzzy Logic System. In: *2018 International Conference on Applied Smart Systems ICASS2018*, Medea, Algeria. November 24–25, 2018.
- [11] A. Morsli, A. Tlemçani, and M. S. Boucherit. Shunt Active Power Filter Based Harmonics Compensation of a Low-Voltage Network Using Fuzzy Logic System. *Nonlinear Dynamics and Systems Theory* **17** (01) (2017) 70–85.
- [12] A. Morsli. Réduction de la pollution des réseaux électriques basses tensions fondée sur les compensateurs actifs : Théorie et réalisation. *Thèse de Doctorat en Génie Electrique. Option: Automatique. Ecole Nationale Polytechnique ENP, Algeria*, 2018.
- [13] R. Chibani, E. Berkouk and M. S. Boucherit. Study of a new DC voltage equalising circuit for Five-Level Neutral Point Clamped-Voltage Source Inverter. *Electrical Systems* **07** (02) (2011) 131–148.
- [14] R. S. Herrera, P. Salmeron and H. Kim. Instantaneous reactive power theory applied to active power filter compensation: different approaches, assessment and experimental results. *IEEE Trans. on Industrial Electronics* **55** (01) (2008) 184–196.
- [15] A. Chaoui, J. P. Gaubert and F. Krim. Power quality improvement using DPC controlled three-phase shunt active filter. *Electr. Power Syst. Res.* **80** (2010) 657–666.
- [16] A. Semmah, A. Massoum, H. Hamdaoui and P. Wira. Comparative Study of PI and Fuzzy DC Voltage Control for a DPC- PWM Rectifier. *Przeegląd Elektrotechniczny* **87** (10) (2011) 355–359.
- [17] A. Chaoui, J. P. Gaubert and A. Bouafia. Direct Power Control Switching Table Concept and Analysis for Three-phase Shunt Active Power Filter. *Journal of Electrical Systems* **09** (01) (2013) 52–65.